nature geoscience
SUPPLEMENTARY INFORMATION
DOI: 10.1038/NGEO962

SUPPLEMENTARY MATERIAL for: "Glacier advance in southern middle latitudes during the Antarctic Cold Reversal" by A.E. Putnam *et al.*

1.0 Supplementary Note: Debate over the signature of late-glacial climate change in the Southwestern Pacific

The expression of late-glacial climate in the middle latitudes of the Southern Hemisphere is uncertain, particularly in the southwestern Pacific region, north of the East Antarctic ice-core sites. The timing of a late-glacial reversal (if any) in this region has been the subject of debate for several decades. For example, some sea-surface temperature (SST) proxies from marine cores near New Zealand do not show a distinct late-glacial reversal[1,2], whereas others register pronounced cooling coincident with the ACR[3,4]. Similar contrasts appear in terrestrial palaeoecological records from New Zealand. Some pollen and chironomid assemblages imply a late-glacial reversal broadly coincident with the ACR[5-7], whereas other pollen records show an indistinct reversal that aligns imprecisely with the ACR[8,9]. Still other pollen curves show no late-glacial reversal at all[10]. Similar disparities exist regarding Patagonian late-glacial climate inferred from terrestrial archives. Some terrestrial proxy records are taken as being variably consistent with ACR cooling (e.g., refs. 11-13), however in most cases temporal resolution and/or the level of robustness of proxy inferences are insufficient to address definitively problems associated with the timing of late-glacial climate change. In particular, combined systematic and analytical uncertainties attending cosmogenic nuclide chronologies could be 14% or more in South America[14], thus precluding confident attribution of glacier activity to specific millennial climate events until local production-

DOI: 10.1038/NGEO962

rate calibration studies have been conducted. Additional robust proxies for atmospheric temperature are necessary to resolve this debate.

2.0 Supplementary Note: Setting

An overview of the geologic, tectonic and climatic setting of the Lake Pukaki catchment is provided in the supporting online material of Schaefer *et al.*[15]. In summary, the northeast-southwest-trending Southern Alps, South Island, New Zealand result from ongoing oblique collision of the Indo-Australian and Pacific plates. The highest parts of the mountain chain support an extensive system of alpine glaciers. Present-day glaciers of the Southern Alps are subject to an orographic precipitation regime under which they receive at least 10 m yr^{-1} precipitation [water equivalent; ref. 16] near the Main Divide, with precipitation totals declining exponentially with distance to the east. High mass flux and short response times characterize New Zealand glaciers located close to the Main Divide, enhancing their sensitivity to relatively rapid (i.e., decadal) perturbations in air temperature[16-21]. There are over 3100 extant glaciers in the Southern Alps today[22], and deeply dissected terrain with an abundance of glacial landforms indicates multiple previous episodes of more extensive glaciation on either side of the Main Divide[23].

South Island, New Zealand lies in the path of the southern westerly wind belt and astride the subtropical front, which marks the northern boundary of the Southern Ocean[2]. The glaciers of the Southern Alps, New Zealand, are thus well situated to provide a sensitive record of atmospheric temperature at the nexus of the important oceanographic and atmospheric fronts near South Island[16,20,24]. When it lay at the position of the Birch Hill moraines, the 'Pukaki glacier' drained southward from the highest sector of the main mountain divide of the Main Divide of the Southern Alps and was more than 40 km long.

Mueller, Hooker, Tasman, and Murchison Glacier tributaries, in addition to several smaller valley glaciers, fed the former glacier tongue that extended to the Birch Hill moraines[25,26]. When at the Birch Hill moraines, the former Pukaki glacier had a catchment of about 595 km^2 (consistent with ref. 25) and fluctuations of its ice margin reflected responses to climate signals integrated over the wide areal and altitudinal extent of its Southern Alps catchment (Fig. 2 in main text). Porter[25] estimated that a snowline about 500 ± 50 m below the AD1975 value was necessary to produce the ice tongue that extended from the Main Divide to the Birch Hill moraines. Assuming a lapse rate of 6°C km^{-1} and no change in accumulation, this equates to a temperature about 3°C cooler than modern values.

The Birch Hill and Macaulay study areas are in a region of well-indurated quartzofeldspathic 'greywacke' sandstone and 'argillite' mudstone[27]. Rockfalls and landslides are major contributors of sediment to the glacier and river systems of the Southern Alps[28], and this is the origin of much of the rock material and large boulders that are deposited as moraines[15,29].

Speight[30] originally described the Birch Hill moraine complex as the 'type landform association' of moraines located about two-thirds the distance upvalley between the full-glacial ('Pukaki Landform Association') and Late Holocene moraine ridges. McGregor[31] referred to the Birch Hill landform association as the 'Birch Hill Formation,' and proposed correlations to several other moraines in mountain regions southeast of the Main Divide exhibiting a similar degree of weathering and soil development, and located in similar relative positions upvalley of moraines deposited during the LGM. Among those correlated to the Birch Hill 'type locality' by McGregor[31] were the 'mid-Macaulay

DOI: 10.1038/NGEO962

moraines,' located ~50 km to the northeast, described below. Correlation to the Waiho Loop moraine of Westland has also been suggested[32-34]. Although the reliability of geomorphic correlations is a matter of debate, moraines in this general mid- to upper valley setting are common through the higher parts of the Southern Alps and have been assigned a late-glacial age[27].

The Birch Hill moraines comprise lateral moraine complexes on both sides of the Tasman valley (Fig. S1). The main outer ridge is the most prominent and continuous and was designated as 'Birch Hill I' by McGregor[31], while the main body of inner moraines was identified as 'Birch Hill II' (Fig. 1 in main text). Terminal moraines are not exposed because the valley floor is an aggrading Holocene alluvial floodplain prograding into post-LGM Lake Pukaki. The outer margin of the lateral moraine belts on both valley flanks is marked by the prominent sharp-crested Birch Hill I ridge that is 4 to 6 m in relief, with an overall down-valley gradient of 0.034 (~2°). The left-lateral outer moraine ridge abuts the valley wall in the north and glacially molded bedrock in the south (Fig. S2a). The Birch Hill I right-lateral ridge abuts subdued glaciogenic landforms that we infer were formed during retreat of the Pukaki glacier from its LGM position (Fig. S1b). We infer the sharp geomorphologic contrast between these outboard landforms and the sharply expressed Birch Hill moraines indicates that the outer Birch Hill moraine ridge was constructed at a robust glacier margin, at the culmination of a re-advance of the Pukaki glacier.

The mid-Macaulay terminal moraines lie about midway between the mouth and head of the Macaulay River valley, a tributary of Lake Tekapo (Fig. S2). When it sat at the mid-Macaulay moraines, the former Macaulay glacier ice-tongue was 10 km long[35],

and drained a 33 km^2 catchment (Fig. 2 in main text). The mid-Macaulay moraine set comprises three terminal ridges that are well preserved on the eastern valley side, but overrun by snow-avalanche talus[35] and a large debris-flow deposit to the west[14]. The most prominent ridge is set in the middle of the sequence and contains boulders amenable for surface-exposure dating. On the eastern end of this prominent mid-Macaulay terminal moraine is an outwash channel graded to the ice-contact slope of that moraine; thus the outwash must have been produced contemporaneously with moraine formation. Sharp-crested terminal moraines abutting subdued recessional topography, as well as well-developed aggradational glaciofluvial deposits, suggests that the mid-Macaulay moraines were deposited at the culmination of a glacier advance.

In austral summer 2009 we conducted a reconnaissance moraine-dating survey in the Macaulay valley and sampled the three best boulders we could find on the mid-Macaulay moraines. Each boulder had been deposited in an ice-proximal position while also being unambiguously remote from the debris-flow area west of the Macaulay River. Surface-exposure dating results for these boulders are given in Tables S1 and S2.

3.0 Supplementary Methods

3.1 Sample collection and assumptions

Our sampling criteria and methods follow those described in ref. 14. The lateral moraines on the western, right-lateral flank of the Pukaki valley include numerous large boulders suitable for surface-exposure dating. Likewise, boulders occur on the mid-Macaulay terminal ridges. Boulders chosen for sampling are embedded in or resting in stable positions on Birch Hill and mid-Macaulay moraine complex (Fig. S3). All were

DOI: 10.1038/NGEO962

from moraine ridge crests, except for two of the Macaulay samples, which were embedded in the floor of a meltwater channel through the middle moraine ridge, within 20 m of the ice-contact face. At the locations where boulders were sampled, the landforms show no indication of post-depositional landform modification, such as slumping, gully erosion or fluvial fan deposition. In this part of the Southern Alps, winter snow lies persistently for several months only above ~1500 meters above sea level (m a.s.l.). At the relatively low elevations of the sample sites (<780 and <1,070 m a.s.l. for the Birch Hill and mid-Macaulay samples, respectively), contemporary winter snow cover is slight, with a 1 m snowfall being an exceptional event and melting within a few weeks. For most of the winter, moraines are free of snow. Thus, we assume that the effect of snow cover on ^{10}Be production is negligible.

We collected most samples from the center of the top, level, surfaces of boulders standing 45 to 400 cm above the ground. We sampled only surfaces that were free of any visual indications of spalling, fracturing, rainwater pooling, or exfoliation. The greywacke of the central Southern Alps is generally resistant to granular erosion[36], so we follow Schaefer *et al.*[15] and assume that erosion is close to zero for the timescales considered here. Since the local ^{10}Be production-rate calibration site is of similar age, and located in a similar climate to the Birch Hill moraines (and adjacent to the mid-Macaulay moraines), any minor effects of erosion (for which no correction was made at the calibration site) have been integrated into the production-rate derivation.

We did not apply any corrections for tectonic or glacioisostatic uplift. Although the Southern Alps are currently experiencing differential uplift, the Birch Hill moraines lie in a similar tectonic setting to that of the ^{10}Be production-rate calibration site. The

mid-Macaulay moraines are adjacent to the calibration site. The uplift rate at the calibration site is estimated to be 2 ± 1 mm yr^{-1} (ref. 14), though no correction was made for uplift. Thus, any effect of vertical rise has already been integrated into the production rate and therefore requires no additional correction.

We measured dimensions (length, width, and heights of four sides) of each boulder sampled, and measured the location and elevation relative to the WGS 1984 datum with a Trimble ProXH differential GPS receiver. Coordinates were corrected against data collected by a fixed base station at the Mount John Observatory, ~35 km east of the Birch Hill moraine and ~47 km south of the mid-Macaulay moraines. Elevations were converted to meters a.s.l. Horizontal and vertical uncertainties (1σ) ranged from ~0.1 to 0.2 m and 0.1 to 0.9 m a.s.l., respectively. We measured topographic shielding and surface dip using compass and clinometer, and each boulder and sample site was described, drawn, and photographed from multiple angles.

3.2 ^{10}Be laboratory procedures, analytical techniques, and age calculations

All samples were processed for ^{10}Be measurement at the Lamont-Doherty Earth Observatory (LDEO) Cosmogenic Nuclide Laboratory, following ref. 15, and using the methods described in detail at http://www.ldeo.columbia.edu/tcn/. Beryllium ratios were measured at the Lawrence-Livermore CAMS facility. ^{10}Be/^{9}Be ratios of samples and blanks analyzed before AD2007 were measured relative to the KNSTD standard, and those analyzed during or after AD2007 were measured relative to the 07KNSTD. Ratios measured relative to KNSTD standard were subsequently normalized to the 07KNSTD

DOI: 10.1038/NGEO962

standard by correcting by a factor of 0.9042 (ref. 37). All procedural blanks except two returned $^{10}Be/^{9}Be$ ratios less than 10^{-15}. Blank corrections were generally less than 1%.

We calculated surface-exposure ages using the local New Zealand ^{10}Be production rates of Putnam *et al.*[14] and five standard scaling models of Lal[38] as modified by Stone[39] (abbreviated 'St' after ref. 40), Desilets *et al.*[41] ('De'); Dunai[42] ('Du'); Lifton *et al.*[43] ('Li'); and a time-dependent version of the 'St' scaling ('Lm'[40]). The time-dependent scaling models (De, Du, Li, and Lm) incorporate a high-resolution version of the geomagnetic framework implemented by Balco *et al.*[40], adapted from Lifton *et al.*[44], following Putnam *et al.*[14]. We discuss ages based on the 'Lm' method because that scaling model produces ages that agree best with limiting radiocarbon data from the Boundary Stream production-rate test site ~25 km south of the Birch Hill moraines[14]. We note that all scaling models yield ages that agree to within ~1.2% (1σ) at the Birch Hill and mid-Macaulay moraines, with the Lm method giving the youngest age of the time-dependent methods. All scaling models produce ages that support our final conclusions. Finally, all ages are interpreted as follows. Since salient moraine boulders are among the final glaciogenic debris deposited on a moraine, we regard each exposure age as representing the culmination of moraine construction at the glacier margin.

3.3 ^{10}Be data

Surface-exposure sample details and nuclide concentrations are given in Table S1, and exposure ages are in Table S2. For comparison to calibrated radiocarbon ages, surface-exposure ages have been referenced to years before Common Era (CE) 1950 (i.e., 'cal. yrs BP'; expressed here and in the main text just as 'yrs') by subtracting 53, 56, 57,

and 59 years from exposure ages determined from samples collected in CE2003, CE2006, CE2007, and CE2009 respectively. Ages are presented as probability density plots (i.e., 'camelplots') for the 'outboard', 'Birch Hill I' (main outer ridge), 'Birch Hill II' (i.e., inner recessional ridges), and 'mid-Macaulay moraine', respectively, in Fig. S4. The data set contains one anomalously old age, BH-07-11 (15,820 ± 1,580 yrs), which lies on the Birch Hill I ridge. We consider this age an outlier since it is more than three standard deviations beyond the mean age of the data set. The BH-07-11 age is also considered an outlier according to the Grubbs[45] test ($P < 0.01$). We therefore did not include this sample in the mean or uncertainty of the overall Birch Hill I age distribution.

3.4 Canavan's Knob radiocarbon calibration

To promote comparison between ^{10}Be and ^{14}C ages, the radiocarbon ages of Denton and Hendy[46] and Turney *et al.*[47] were converted to calendar ages using the R_Combine function of the OxCal 4.1 program[48] (http://c14.arch.ox.ac.uk/oxcal.html) and the IntCal09 atmospheric radiocarbon calibration curve of Reimer *et al.*[49] We combined the radiocarbon data of Denton and Hendy[46] and Turney *et al.*[47] to calculate an average maximum-limiting calendar age for the Canavans Knob till. Converted calendrical ages are 13,030 ± 40 cal. yrs BP (n=36) and 12,950 ± 90 cal. yrs BP (n=4) for the data sets of Denton and Hendy[46] and Turney *et al.*[47], respectively. Both data sets agree, and each affords a maximum-limiting calendar age for the Canavans Knob till. Combining the radiocarbon data of Denton and Hendy[46] and those preferred by Turney *et al.*[47] yield an average maximum limiting calendar age for the Canavans Knob till of 13,030 ± 40 cal.yrs BP (n=38; Table S3). We did not apply the 'transport' correction

DOI: 10.1038/NGEO962

suggested by Denton and Hendy[46] because subsequent observations have identified bark that would most likely not remain if transported over long distances[47]. Radiocarbon dates from bark accord with the mean value of the data set, affirming a proximal source for the wood buried beneath the Canavans Knob till[47].

While entirely compatible with the Birch Hill results, recent hypotheses have called into question the climatic interpretation of till at Canavans Knob [i.e., ref. 50], and there is disagreement about the age and significance of the nearby Waiho Loop moraine[1,46,50]. A recent modeling test[51] of proposed non-climatic drivers (i.e., a large rock avalanche[50]) favored the classical interpretation that the advance of the Franz Josef Glacier to the Waiho Loop moraine was in response to climatic forcing. Thus we tentatively adopt this climatic interpretation in our assessment of the radiocarbon ages of Denton and Hendy[46] and Turney *et al.*[47] We acknowledge however that further work is needed to evaluate these issues.

3.5 Constructing a relative time-distance diagram for the Pukaki-Tasman valley

The relative time-distance diagram shown in Fig. 3 in the main text is based on glacial geomorphological interpretations and ^{10}Be surface-exposure ages of the Birch Hill moraines from this study, as well as pertinent previously published ^{14}C and ^{10}Be data. We adopted an age of 18,350 ± 390 yrs for the onset of the termination (i.e., the time at which the last full-glacial moraines were abandoned) determined from the Pukaki right-lateral ('Boundary Stream') moraine ridges by Putnam *et al.*[14]. This age is a refinement of the Schaefer *et al.*[26] dataset. The moraine ridges dated by Putnam *et al.*[14] can be traced to the innermost ridges sampled by Schaefer *et al.*[26], and ages reported in both studies

show close agreement when ^{10}Be concentrations of Schaefer *et al.*[26] are normalized to the 07KNSTD standard and when calculated using the New Zealand production rate[14]. We referenced the exposure ages to calendar yrs BP (see above), and used an age uncertainty based on the standard error of the mean propagated with a production-rate uncertainty of 2.1%.

An IntCal09[49] calibrated radiocarbon age of 16,370 ± 460 cal. yrs BP (determined using the OxCal 4.0.1 program) obtained from retreat landforms at the head of Lake Pukaki[52] places a minimum age on the retreat of the Pukaki glacier to a position that was ~55% of its full-glacial length. We adopt this age as a limiting control point for the deglaciation of the Pukaki glacier up-valley toward the Birch Hill moraine. Finally, we use the mean ^{10}Be ages for the 'outer ridge' (14,090 yrs) and 'Birch Hill I' (12,970 yrs) ridges determined in this study. For the 'Birch Hill II' ridges, we chose as a representative age the younger error bound (12,820 yrs) of the mean age (13,120 ± 300 yrs).

Since the Birch Hill terminal moraines are not preserved, we constructed a longitudinal profile of the Pukaki-Tasman valley to assess height differences between lateral moraines associated with each dated ice margin. The profile (Fig. S5) is drawn from the névé of the Tasman Glacier, down the axes of the Tasman Glacier, the Tasman valley and the Lake Pukaki basin, to the Lake Pukaki outlet. Topographic profiles are estimated using 20-m interval contours on published 1:50 000 scale topographic maps. The mid 20th century terminus of the Tasman Glacier, now the outlet of developing proglacial Tasman Lake, is the reference mark for down-valley distances. At Lake Pukaki, we show the original natural lake level (pre-1951) and its modern maximum level

DOI: 10.1038/NGEO962

following impoundment in 1979 for hydroelectric storage. The subsurface geometries of Tasman Glacier and Tasman Lake are based on data from refs. 53 and 54. The base of glacial deposits near Lake Pukaki comes from ref. 55. The elevation of the ~16,400 yr ice-contact kame terrace/moraine at the head of Lake Pukaki equates to a ~400 m ice-surface lowering from the ~18,300 yr (i.e., innermost) LGM ice margin ('LGM ice surface').

The crest of the Birch Hill I moraine represents approximately 500 m of ice-surface lowering from the LGM ice surface. Extrapolations indicate that the late Holocene ice position equates to a surface lowering of about 450 m from the Birch Hill ice surface level. Thus the 150 m of ice-surface lowering represented by the Birch Hill recessional moraine sequence examined in this study equates to about 1/3 of the ice level change between late-glacial and late Holocene time. Considering just ice levels, the step-wise overlap between the LGM, Birch Hill and late Holocene profiles furnishes indicative values for total post-LGM ice-surface lowering in the Tasman – Pukaki valley system. The Holocene ice surface is about 950 m lower than the LGM termination ice surface, while the Birch Hill ice surface equates to a lowering of ~47% from the LGM level, with the Birch Hill recessional sequence corresponding to a further 16% lowering relative to the LGM ice surface.

Taking into account the Birch Hill moraine gradients and the amount of ice-surface lowering implies to a first approximation that the glacier terminus probably retreated at least ~5 km during construction of the Birch Hill II moraines preserved in our study area (Fig. S5).

4.0 Supplementary Discussion: The role of temperature as the primary driver of New Zealand glacier activity

While atmospheric temperature has been favored as the dominant driver of glacier mass balance in the Southern Alps [e.g., refs. 15,17,19-21,26,46,56-60], it has also been suggested that precipitation[61] and rock avalanches[29,50,62] have important influences on the behavior of some glacier termini. We follow Schaefer *et al.*[15] in preferring to rely upon the well-established empirical links between atmospheric temperature and glacier mass-balance, and consider that atmospheric temperature is most likely the primary control on ice-margin fluctuation over the timescales considered here.

DOI: 10.1038/NGEO962

Supplementary References

1 Barrows, T. T., Lehman, S. J., Fifield, L. K. & Deckker, P. D. Absence of cooling in New Zealand and the adjacent ocean during the Younger Dryas chronozone. *Science* **318**, 86-89 (2007).

2 Carter, L. & Cortese, G. Change in the Southern Ocean: Responding to Antarctica. *PAGES News* **17**, 30-31 (2009).

3 Pahnke, K. & Zahn, R. Southern hemisphere water mass conversion linked with North Atlantic climate variability. *Science* **307**, 1741-1746 (2005).

4 Calvo, E., Pelejero, C., Deckker, P. D. & Logan, G. A. Antarctic deglacial pattern in a 30 kyr record of sea surface temperature offshore South Australia. *Geophysical Research Letters* **34**, doi:10.1029/2007GL029937 (2007).

5 Alloway, B. V. *et al.* Towards a climate event stratigraphy for New Zealand over the past 30 000 years (NZ-INTIMATE project). *Journal of Quaternary Science* **22**, 9-35 (2007).

6 Hajdas, I., Lowe, D. J., Newnham, R. M. & Bonani, G. Timing of the late-glacial climate reversal in the Southern Hemisphere using high-resolution radiocarbon chronology for Kaipo bog, New Zealand. *Quaternary Research* **65**, 340-345 (2006).

7 Vandergoes, M. J., Dieffenbacher-Krall, A. C., Newnham, R. M., Denton, G. H. & Blaauw, M. Cooling and changing seasonality in the Southern Alps, New Zealand during the Antarctic Cold Reversal. *Quaternary Science Reviews* **27**, 589-601 (2008).

8 McGlone, M. S., Turney, C. S. M. & Wilmshurst, J. M. Late-glacial and Holocene vegetation and climatic history of the Cass Basin, central South Island, New Zealand. *Quaternary Research* **62**, 267-279 (2004).

9 Turney, C. S. M., McGlone, M. S. & Wilmshurst, J. M. Asynchronous climate change between New Zealand and the North Atlantic during the last deglaciation. *Geology* **31**, 223-226 (2003).

10 Singer, C., Shulmeister, J. & B. McLea. Evidence against a significant Younger Dryas cooling event in New Zealand. *Science* **281**, 812-814 (1998).

11 Fogwill, C. J. & Kubik, P. W. A glacial stage spanning the Antarctic Cold Reversal in Torres del Paine (51°S), Chile, based on preliminary cosmogenic exposure ages. *Geografiska Annaler* **87A**, 403-408 (2005).

12 Moreno, P. I., Kaplan, M.R., François, J.P., Villa-Martínez, R., Moy, C.M., Stern, C.R., Kubik, P.W. Renewed glacial activity during the Antarctic Cold Reversal and persistence of cold conditions until 11.5 ka in southwestern Patagonia. *Geology* **37**, 375-378 (2009).

13 Rodbell, D. T., Smith, J. A. & Mark, B. G. Glaciation in the Andes during the Lateglacial and Holocene. *Quaternary Science Reviews* **28**, 2165-2212 (2009).

14 Putnam, A. E. *et al.* In situ cosmogenic ^{10}Be production-rate calibration from the Southern Alps, New Zealand. *Quaternary Geochronology* **5**, 392-409 (2010).

15 Schaefer, J. M. *et al.* High-frequency Holocene glacier fluctuations in New Zealand differ from the northern signature. *Science* **324**, 622-625 (2009).

16 Lamont, G. N., Chinn, T. J. H. & Fitzharris, B. B. Slopes of glacier ELAs in the Southern Alps of New Zealand in relation to atmospheric circulation patterns. *Global and Planetary Change* **22**, 209-219 (1999).
17 Anderson, B., Lawson, W., Owens, I. & Goodsell, B. Past and future mass balance of 'Ka Roimata o Hine Hukatere' Franz Josef Glacier, New Zealand. *Journal of Glaciology* **52**, 597-607 (2006).
18 Oerlemans, J. Climate sensitivity of glaciers in southern Norway: application of an energy-balance model to Nigardsbreen, Hellstugubreen and Alfotbreen. *Journal of Glaciology* **38**, 223-232 (1992).
19 Anderson, B. *et al.* Climate sensitivity of a high-precipitation glacier in New Zealand. *Journal of Glaciology* **56**, 114-128 (2010).
20 Clare, G. R., Fitzharris, B. B., Chinn, T. J. H. & Salinger, M. J. Interannual variation in end-of-summer snowlines of the Southern Alps of New Zealand, and relationships with Southern Hemisphere atmospheric circulation and sea surface temperature patterns. *International Journal of Climatology* **22**, 107-120 (2002).
21 Oerlemans, J. Climate sensitivity of Franz Josef Glacier, New Zealand, as revealed by numerical modelling. *Arctic and Alpine Research* **29**, 233-239 (1997).
22 Chinn, T. J. H. New Zealand glacier response to climate change of the past 2 decades. *Global and Planetary Change* **22**, 155-168 (1999).
23 Suggate, R. P. Late Pliocene and Quaternary glaciations of New Zealand. *Quaternary Science Reviews* **9**, 175-197 (1990).
24 Hooker, B. L. & Fitzharris, B. B. The correlation between climatic parameters and the retreat and advance of Franz Josef Glacier, New Zealand. *Global and Planetary Change* **22**, 39-48 (1999).
25 Porter, S. C. Equilibrium-line altitudes of Late Quaternary glaciers in the Southern Alps, New Zealand. *Quaternary Research* **5**, 27-47 (1975).
26 Schaefer, J. M. *et al.* Near-synchronous interhemispheric termination of the last glacial maximum in mid-latitudes. *Science* **312**, 1510-1513 (2006).
27 Cox, S. C. & Barrell, D. J. A. Geology of the Aoraki area. *Institute of Geological and Nuclear Sciences 1:250,000 Geological Map 15 GNS Science, Lower Hut, New Zealand*, 1 sheet and 71 pp. (2007).
28 Whitehouse, I. E. & Griffiths, G. A. Frequency and hazard of large rock avalanches in the central Southern Alps, New Zealand. *Geology* **11**, 331-334 (1983).
29 Shulmeister, J., Davies, T. R., Evans, D. J. A., Hyatt, O. M. & Tovar, D. S. Catastrophic landslides, glacier behaviour and moraine formation - a view from an active plate margin. *Quaternary Science Reviews* **28**, 1085-1096 (2009).
30 Speight, J. G. Late Pleistocene historical geomorphology of the Lake Pukaki area, New Zealand. *New Zealand Journal of Geology and Geophysics* **6**, 160-188 (1963).
31 McGregor, V. R. Holocene moraines and rock glaciers in the central Ben Ohau Range, South Canterbury. *Journal of Glaciology* **6**, 737-748 (1967).
32 Burrows, C. J. Radiocarbon dates for post-Otiran glacial activity in the Mount Cook region, New Zealand. *New Zealand Journal of Geology and Geophysics* **23**, 239-248 (1980).

DOI: 10.1038/NGEO962

33 Suggate, R. P. The upper boundary of the Hawera Series. *Transactions of the Royal Society of New Zealand Geology* **1**, 11-16 (1961).

34 Mercer, J. H. The age of the Waiho Loop terminal moraine, Franz Josef Glacier, Westland. *New Zealand Journal of Geology and Geophysics* **31**, 95-99 (1988).

35 McSaveney, M. J. & Whitehouse, I. E. An early Holocene glacial advance in the Macaulay River valley, central Southern Alps, New Zealand. *New Zealand Journal of Geology and Geophysics* **32**, 217-223 (1989).

36 Birkeland, P. W. Subdivision of Holocene glacial deposits, Ben Ohau Range, New Zealand, using relative-dating methods. *Geological Society of America Bulletin* **93**, 443-449 (1982).

37 Nishiizumi, K. *et al.* Absolute calibration of ^{10}Be AMS standards. *Nuclear Instruments and Methods in Physics Research B* **258**, 403-413 (2007).

38 Lal, D. Cosmic-ray labeling of erosion surfaces: in situ nuclide production rates and erosion models. *Earth and Planetary Science Letters* **104**, 424-439 (1991).

39 Stone, J. O. Air pressure and cosmogenic isotope production. *Journal of Geophysical Research* **105**, 23753-23759 (2000).

40 Balco, G., Stone, J. O., Lifton, N. A. & Dunai, T. J. A complete and easily accessible means of calculating surface exposure ages or erosion rates from ^{10}Be and ^{26}Al measurements. *Quaternary Geochronology* **4** (2008).

41 Desilets, D., Zreda, M. & Prabu, T. Extended scaling factors for in situ cosmogenic nuclides: new measurements at low latitude. *Earth and Planetary Science Letters* **246**, 256-276 (2006).

42 Dunai, T. Influence of secular variation of the magnetic field on production rates of in situ produced cosmogenic nuclides. *Earth and Planetary Science Letters* **193**, 197-212 (2001).

43 Lifton, N. *et al.* Addressing solar modulation and long-term uncertainties in scaling secondary cosmic rays for in situ cosmogenic nuclide applications. *Earth and Planetary Science Letters* **239**, 140-161 (2005).

44 Lifton, N., Smart, B. & Shea, M. Scaling time-integrated in situ cosmogenic nuclide production rates using a continuous geomagnetic model. *Earth and Planetary Science Letters* **268**, 190-201 (2008).

45 Grubbs, F. E. Procedures for detecting outlying observations in samples. *Technometrics* **11**, 1-21 (1969).

46 Denton, G. H. & Hendy, C. H. Younger Dryas age advance of Franz Josef Glacier in the Southern Alps of New Zealand. *Science* **264**, 1434-1437 (1994).

47 Turney, C. S. M. *et al.* Redating the advance of the New Zealand Franz Josef Glacier during the Last Termination: evidence for asynchronous climate change. *Quaternary Science Reviews* **26**, 3037-3042 (2007).

48 Bronk Ramsay, C. Oxcal 4.0 Manual. Oxcal Program 4.0.7. (2007).

49 Reimer, P. J., et al. INTCAL09 and MARINE09 radiocarbon age calibration curves, 0-50,000 years cal BP. *Radiocarbon* **51**, 1111-1150 (2009).

50 Tovar, D. S., Shulmeister, J. & Davies, T. R. Evidence for a landslide origin of New Zealand's Waiho Loop moraine. *Nature Geoscience* **1**, 524-526 (2008).

51 Vacco, D. A., Alley, R. B. & Pollard, D. Glacial advance and stagnation caused by rock avalanches. *Earth and Planetary Science Letters* **294**, 123-130 (2010).

52 Moar, N. T. Late Otiran and early Aranuian grassland in central South Isand. *New Zealand Journal of Ecology* **3**, 4-12 (1980).

53 Broadbent, M. Seismic and gravity surveys on the Tasman Glacier 1971-2. *Geophysics Division report no. 91. Department of Scientific and Industrial Research, Wellington, New Zealand.* (1974).

54 Hochstein, M. P. *et al.* Downwasting of the Tasman Glacier terminus, South Island, New Zealand: changes in the terminus region between 1971 and 1993. *New Zealand Journal of Geology and Geophysics* **38**, 1-16 (1995).

55 Kleffmann, S. *et al.* Crustal structure in the central South Island, New Zealand, from the Lake Pukaki seismic experiment. *New Zealand Journal of Geology and Geophysics* **41**, 39-50 (1998).

56 Harrington, H. J. Glacier wasting and retreat in the Southern Alps of New Zealand. *Journal of Glaciology* **2**, 140-144 (1952).

57 Anderson, B. Interactive comment on "Synoptic climate change as a driver of late Quaternary glaciations in the mid-latitudes of the Southern Hemisphere" by H. Rother and J. Shulmeister. *Climate of the Past Discussions* **1**, S161-S167 (2005).

58 Anderson, B. & Mackintosh, A. Temperature change is the major driver of late-glacial and Holocene glacier fluctuations in New Zealand. *Geology* **34**, 121-124 (2006).

59 Burrows, C. J. *Julius Haast in the Southern Alps*. (Canterbury University Press, 2005).

60 Salinger, M. J. On the suggestion of post-1950 warming over New Zealand. *New Zealand Journal of Science* **25**, 77-86 (1982).

61 Rother, H. & Shulmeister, J. Synoptic climate change as a driver of late Quaternary glaciations in the mid-latitudes of the Southern Hemisphere. *Climate of the Past Discussions* **1**, 231-253 (2005).

62 Larsen, S. H., Davies, T. R. H. & McSaveney, M. J. A possible coseismic landslide origin of late Holocene moraines of the Southern Alps. *New Zealand Journal of Geology and Geophysics* **48**, 311-314 (2005).

63 NGRIP_Members. High-resolution record of Northern Hemisphere climate extending into the last interglacial period. *Nature* **431**, 147-151 (2004).

64 Rasmussen, S. O. *et al.* A new Greenland ice core chronology for the last glacial termination. *Journal of Geophysical Research* **111**, D06102 (2006).

65 Lemieux-Dudon, B. *et al.* Consistent dating for Antarctic and Greenland ice cores. *Quaternary Science Reviews* **29**, 8-20 (2010).

66 Calvo, E., Pelejero, C., De Deckker, P. & Logan, G. A. Antarctic deglacial pattern in a 30 kyr record of sea surface temperature offshore South Australia. *Geophysical Research Letters* **34**, L13707 (2007).

67 Lamy, F. *et al.* Antarctic timing of surface water changes off Chile and Patagonian ice sheet response. *Science* **304**, 1959-1962 (2004).

68 Barker, S. *et al.* Interhemispheric Atlantic seesaw response during the last deglaciation. *Nature* **457**, 1097-1102 (2009).

69 Monnin, E. *et al.* Atmospheric CO_2 concentrations over the last glacial termination. *Science* **291**, 112-114 (2001).

DOI: 10.1038/NGEO962

SUPPLEMENTARY FIGURES

Figure S1a. An aerial view northwest toward the upper reaches of the Tasman River valley, showing the prominent left-lateral Birch Hill lateral moraine complex. Aoraki/Mount Cook is the highest peak in the background. Note the molded bedrock topography outboard of the Birch Hill I ridge toward the bottom of the image, and LGM moraines preserved higher on the valley side towards upper right. The boundary between hummocky LGM deglacial moraines and the smoother moraine/kame terrace upslope is interpreted as marking the ~18,300 yr LGM ice surface. This boundary lies 500 ± 20 m above the Birch Hill I ridge.

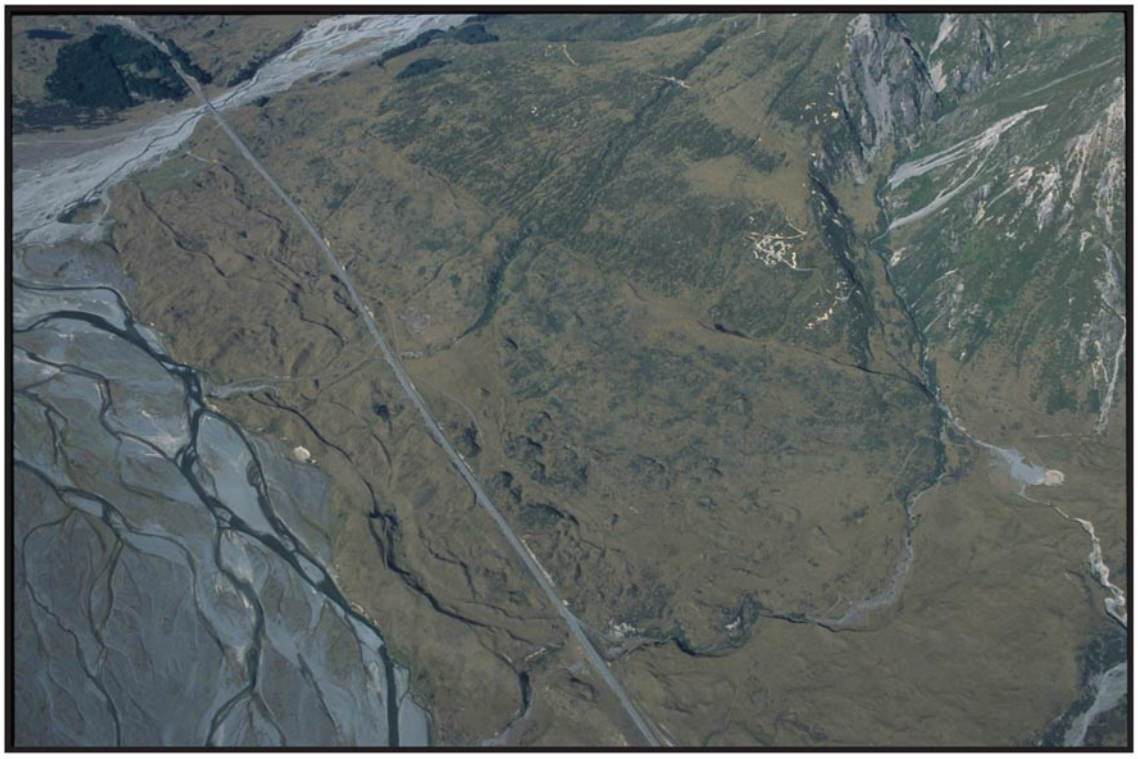

Figure S1b. An aerial view southwest across the right-lateral Birch Hill moraine belt, highlighting the morphological contrast with older subdued moraine topography to the upper right. The Birch Hill I ridge marks the upper limit of the moraine complex, while the Birch Hill II recessional ridges occur lower in the image toward the valley floor.

DOI: 10.1038/NGEO962

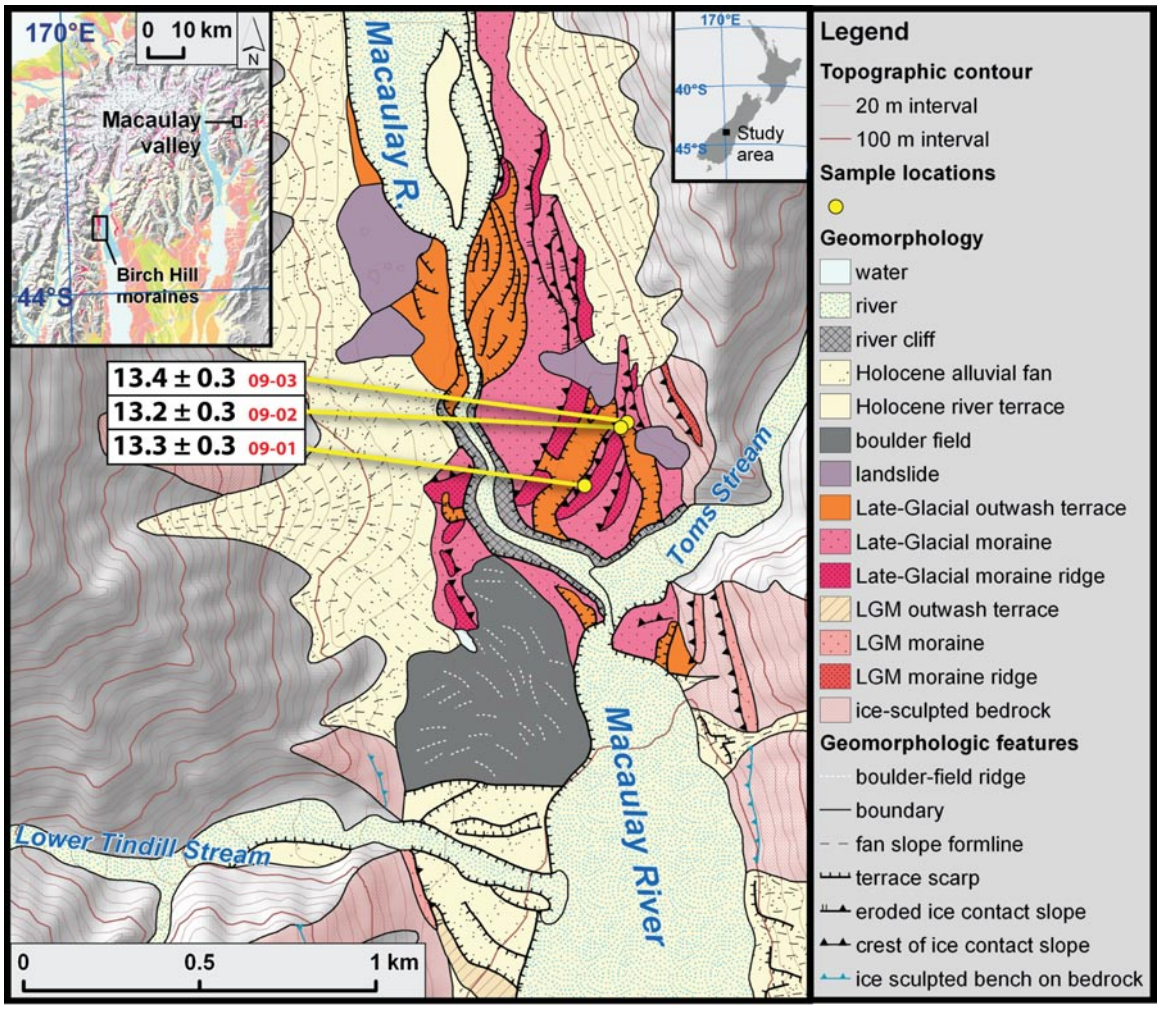

Figure S2. Glacial geomorphic map of the mid-Macaulay moraines. Regional map and legend are inset. Yellow dots indicate surface-exposure sample locations and ages are in white boxes (in kyrs). Figure adapted from Putnam *et al.*[14]

Figure S3. Examples of boulders on the Birch Hill and mid-Macaulay moraines selected for sampling for ^{10}Be measurements. Sample sites are arrowed. Photo **a** looks west across Birch Hill moraine toward Freds Stream valley. In photo **b**, the view is north toward the upper reaches of the Tasman valley. In Photo **c** the view is to the north, with the upper reaches of the Tasman (right) and Hooker (left) valleys visible in the distance. Photo **d** looks to the east, with the upper Pukaki left-lateral moraine ridges, deposited before and during the LGM, defining the background skyline. Photo **e** looks southwest, down the Macaulay valley. Mid-Macaulay terminal moraine ridge is in foreground. Photo **f** looks north up the Macaulay valley. Person (A.M. Doughty) in photos A and D is 1.7 m tall. Person (D.J.A. Barrell) in photo **e** is 1.9 m tall.

DOI: 10.1038/NGEO962

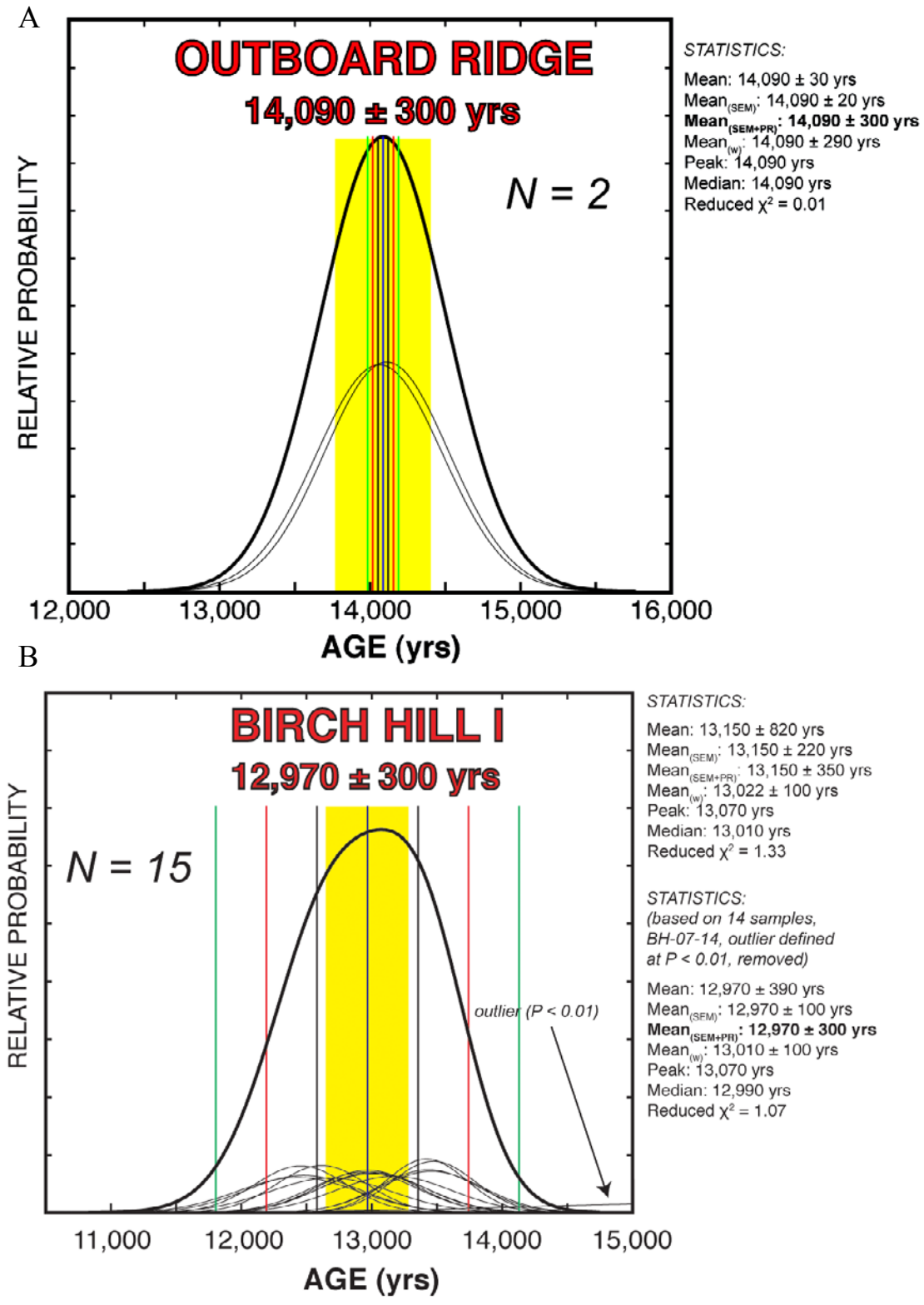

Figure S4. (caption below)

C

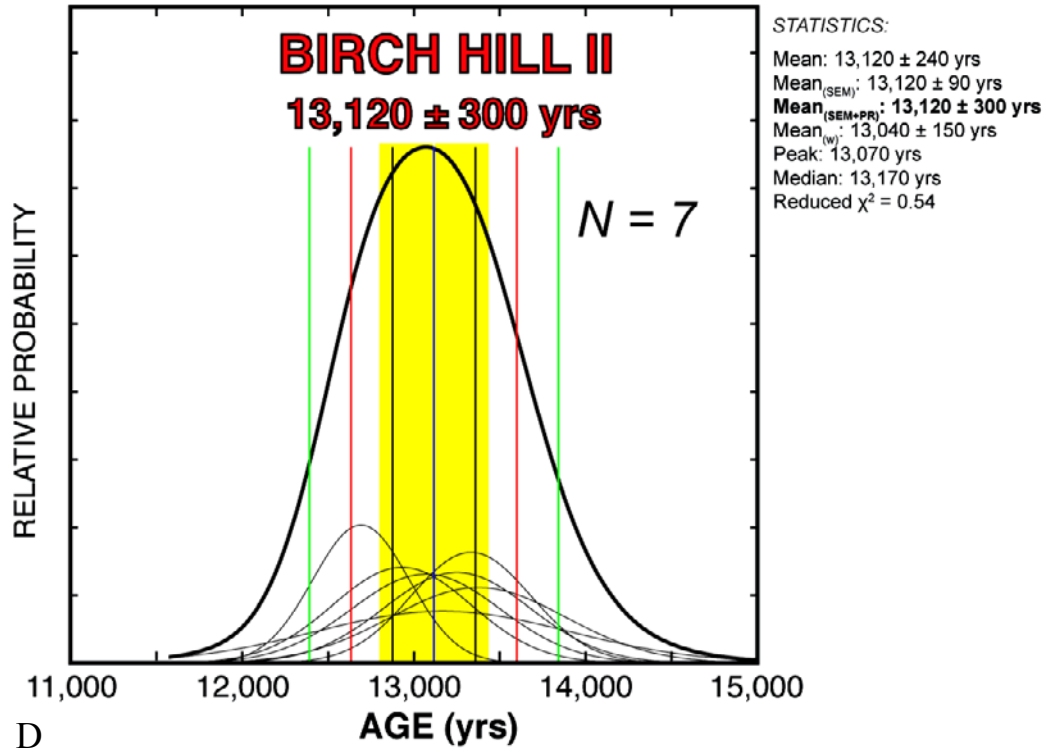

D

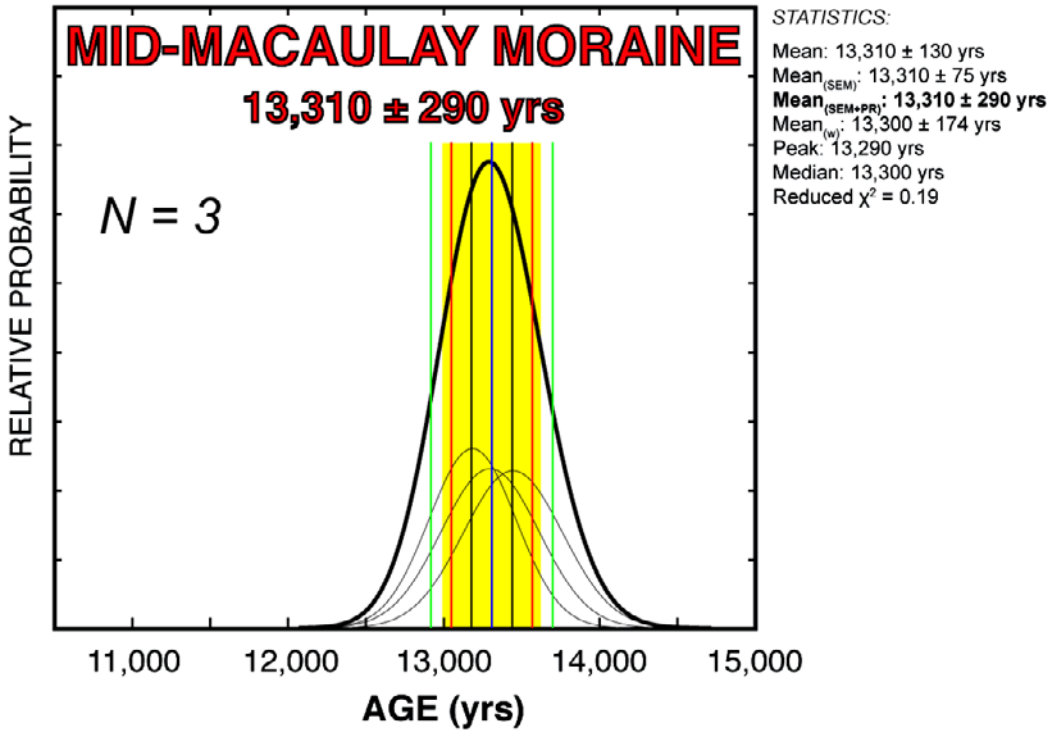

Figure S4 (cont.). Caption on following page.

DOI: 10.1038/NGEO962

Figure S4 (cont.). Probability density plots showing ages of A) outboard Birch Hill moraine ridge, B) the Birch Hill I moraine ridge, C) the Birch Hill II moraine ridges, and D) the mid-Macaulay moraine. Thin lines are Gaussian curves of individual ages and bold lines represent the summed probability of all ages. Black, red, and green vertical lines mark one, two, and three standard deviations, respectively. Middle vertical line denotes the arithmetic mean. The yellow area represents the uncertainty calculated using the standard error of the mean propagated with the production-rate uncertainty (2.1%). Summary statistics are inset.

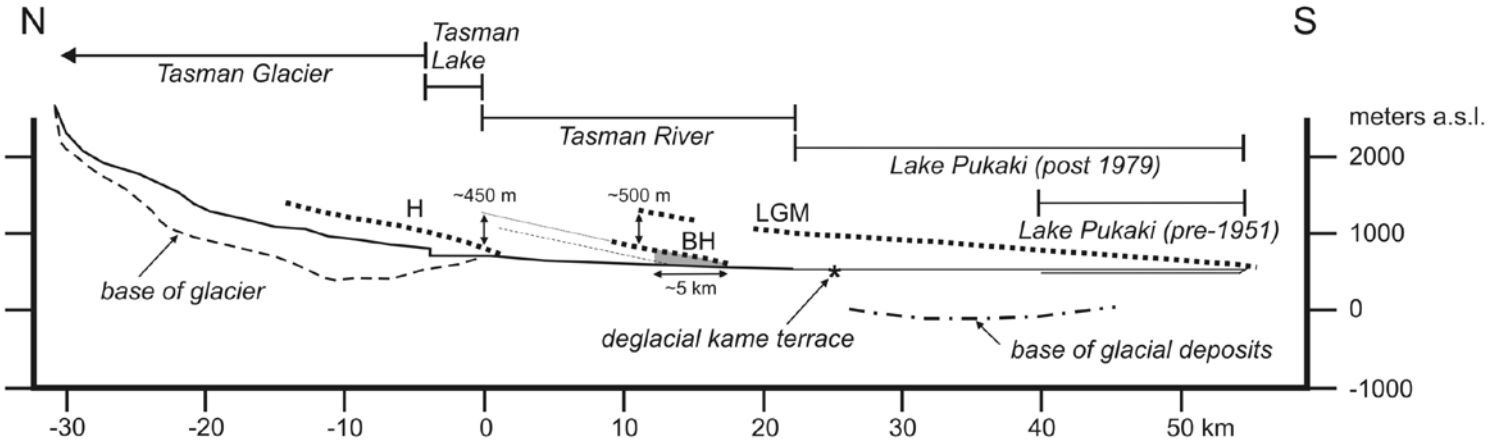

Figure S5. Longitudinal profile of the Tasman-Pukaki valley system. Heavy dotted lines denote the crests of preserved moraine belts. LGM is the final ice position prior to deglacial retreat at the onset of the local termination [~18,300 yrs; ref. 14]. Elevations are based principally on the left-lateral moraine of the Pukaki trough, which is continuous except where interrupted by the Jollie valley at profile distance 15 to 19 km. The deglacial kame moraine has a minimum-limiting age of ~16,400 yrs. The Birch Hill profile (BH) is based mainly on the near-continuous left-lateral moraine. Grey shading shows the area of the right-lateral moraines dated in this study. The extrapolation of the moraine crest to the Tasman Glacier terminus is denoted by the fine dotted line and the extrapolation of the base of the dated sequence by the fine dashed line. H is the late 19th to early 20th century moraine crest of the Tasman Glacier, best preserved in the left-lateral sector of the glacier.

Table S1. Birch Hill moraine surface-exposure sample details and ^{10}Be data.

CAMS laboratory no.	Sample ID	Latitude (DD)	Longitude (DD)	Elevation (m a.s.l.)	Boulder size (L x W x H) (cm)	Sample Thickness (cm)	Shielding correction	Quartz weight (g)	Carrier Added (mg)[a]	^{10}Be/^{9}Be ± 1σ (10^{-14})	[^{10}Be] ± 1σ (10^{4} atoms · g^{-1})	Average ^{9}Be current (μA)[b]	AMS Std[c]
'Outboard' Birch Hill ridge													
BE24215	BH-07-08	-43.854994	170.112755	584.8	670 x 430 x 290	1.51	0.997	10.0037	0.2013	6.78 ± 0.20	9.08 ± 0.26	16.2 (2)	07KNSTD$_{B2,3}$
BE24216	BH-07-09	-43.855111	170.113130	588.6	490 x 290 x 128	2.73	0.991	10.0085	0.2019	6.71 ± 0.20	9.01 ± 0.26	16.9 (2)	07KNSTD$_{B2,3}$
Birch Hill I ridge													
BE23308	BH-06-02	-43.819065	170.106203	747.3	380 x 360 x 205	1.26	0.994	10.3670	0.2037	8.11 ± 0.26	10.65 ± 0.34	13.0 (2)	KNSTD$_{B1}$
BE23309	BH-06-03	-43.823093	170.105082	681.3	480 x 425 x 185	1.92	0.992	10.1113	0.2030	7.13 ± 0.26	9.57 ± 0.35	13.0 (3)	KNSTD $_{B1}$
BE23310	BH-06-04	-43.822836	170.105449	688.8	235 x 180 x 146	1.63	0.990	10.0593	0.2044	7.11 ± 0.20	9.66 ± 0.27	12.7 (3)	KNSTD $_{B1}$
BE23311	BH-06-05	-43.814750	170.105398	765.6	820 x 440 x 195	2.25	0.998	10.2014	0.2010	7.85 ± 0.28	10.34 ± 0.36	13.4 (3)	KNSTD $_{B1}$
BE23312	BH-06-06	-43.811233	170.104487	765.1	270 x 255 x 108	1.79	0.995	10.0882	0.2035	7.99 ± 0.25	10.77 ± 0.33	13.7 (2)	KNSTD $_{B1}$
BE23313	BH-06-07	-43.808384	170.102947	772.9	530 x 250 x 170	1.15	0.995	10.0974	0.2042	7.86 ± 0.29	10.62 ± 0.39	11.7 (2)	KNSTD $_{B1}$
BE24217	BH-07-10	-43.854687	170.114450	578.7	580 x 530 x 218	1.73	0.997	10.0055	0.2014	6.04 ± 0.17	8.09 ± 0.22	16.1 (3)	07KNSTD$_{B2,3}$
BE24218	BH-07-11	-43.853697	170.114478	577.7	420 x 175 x 128	1.33	0.997	0.7685	0.1716	0.68 ± 0.07	10.18 ± 1.01	15.8 (4)	07KNSTD$_{B2,3}$
BE24219	BH-07-12	-43.853602	170.113740	583.6	210 x 140 x 73	1.83	0.998	10.0035	0.2010	6.24 ± 0.18	8.35 ± 0.25	17.5 (4)	07KNSTD$_{B2,3}$
BE24220	BH-07-13	-43.837554	170.106321	679.1	400 x 170 x 60	1.86	0.993	10.0196	0.2010	7.00 ± 0.16	9.35 ± 0.22	16.5 (3)	07KNSTD$_{B2,3}$
BE24221	BH-07-14	-43.835540	170.106740	674.9	280 x 200 x 80	1.68	0.998	9.3105	0.2015	6.48 ± 0.15	9.33 ± 0.21	19.3 (3)	07KNSTD$_{B2,3}$
BE24222	BH-07-15	-43.835513	170.106733	674.9	300 x 140 x 58	2.01	0.998	5.7973	0.1914	4.16 ± 0.14	9.14 ± 0.31	15.7 (3)	07KNSTD$_{B2,3}$
BE24223	BH-07-16	-43.835497	170.106213	671.5	170 x 130 x 78	1.42	0.995	10.012	0.2011	6.96 ± 0.20	9.31 ± 0.26	17.4 (2)	07KNSTD$_{B2,3}$
BE24224	BH-07-17	-43.833953	170.105455	674.3	760 x 430 x 195	1.35	0.994	9.0703	0.2014	6.08 ± 0.19	8.99 ± 0.28	16.4 (2)	07KNSTD$_{B2,3}$
BE24225	BH-07-18	-43.833708	170.105528	673.2	950 x 600 x 275	1.11	0.996	10.0215	0.2014	7.00 ± 0.20	9.37 ± 0.27	16.3 (2)	07KNSTD$_{B2,3}$

DOI: 10.1038/NGEO962

Table S1 (continued).

CAMS laboratory no.	Sample ID	Latitude (DD)	Longitude (DD)	Elevation (m a.s.l.)	Boulder size (L x W x H) (cm)	Sample Thickness (cm)	Shielding correction	Quartz weight (g)	Carrier Added (mg)[a]	$^{10}Be/^{9}Be \pm 1\sigma$ (10^{-14})	$[^{10}Be] \pm 1\sigma$ (10^{4} atoms · g^{-1})	Average ^{9}Be current (μA)[b]	AMS Std[c]
Birch Hill II ridges													
BE23314	BH-06-09	-43.808516	170.114376	634.9	560 x 500 x 230	1.39	0.994	1.2335	0.1828	0.99 ± 0.06	9.81 ± 0.55	11.6 (4)	$KNSTD_{B1}$
BE23315	BH-06-10	-43.812393	170.114462	607.6	250 x 240 x 110	1.94	0.995	10.0197	0.2025	7.02 ± 0.24	9.48 ± 0.31	12.7 (3)	$KNSTD_{B1}$
BE23316	BH-06-11	-43.816018	170.114640	612.3	140 x 137 x 101	2.35	0.996	10.6883	0.1670	9.01 ± 0.28	9.41 ± 0.29	12.6 (2)	$KNSTD_{B1}$
BE23317	BH-06-12	-43.816755	170.111584	629.6	380 x 260 x 126	1.62	0.995	9.9945	0.1952	7.59 ± 0.29	9.91 ± 0.38	11.5 (3)	$KNSTD_{B1}$
BE23318	BH-06-13	-43.824295	170.113626	606.2	250 x 200 x 168	2.31	0.998	5.7132	0.1868	4.40 ± 0.14	9.61 ± 0.31	12.1 (3)	$KNSTD_{B1}$
BE21020	KIWI 631	-43.823802	170.111548	605.5	560 x 530 x 250	3.10	0.995	15.1288	0.2513	8.63 ± 0.22	9.58 ± 0.25	20.5 (2)	$KNSTD_{B4}$
BE28319	KIWI 632	-43.820842	170.114721	603.7	600 x 350 x 350	1.80	0.996	10.3342	0.1821	7.09 ± 0.16	8.31 ± 0.18	18.7 (3)	$07KNSTD_{B5,6}$
Mid-Macaulay moraine													
BE28331	MR-09-01	-43.570988	170.609952	1064.4	145 x 135 x 45	1.64	0.976	9.7930	0.1814	10.08 ± 0.24	12.43 ± 0.29	17.9 (2)	$07KNSTD_{B7}$
BE28332	MR-09-02	-43.569452	170.611065	1057.3	250 x 180 x 100	1.74	0.975	7.9676	0.1823	8.03 ± 0.17	12.23 ± 0.26	18.4 (3)	$07KNSTD_{B7}$
BE28333	MR-09-03	-43.569397	170.611232	1056.9	340 x 400 x 110	2.62	0.975	9.8660	0.1827	10.06 ± 0.24	12.40 ± 0.21	20.2 (2)	$07KNSTD_{B7}$

Table S1 (continued).

CAMS laboratory no.	Sample ID	Latitude (DD)	Longitude (DD)	Elevation (m a.s.l.)	Boulder size (L x W x H) (cm)	Sample Thickness (cm)	Shielding correction	Quartz weight (g)	Carrier Added (mg) [a]	$^{10}Be/^{9}Be \pm 1\sigma$ (10^{-14})	$[^{10}Be] \pm 1\sigma$ (10^{4} atoms · g^{-1})	Average ^{9}Be current (μA) [b]	AMS Std [c]
Procedural Blanks													
BE23319	Blank 01 Dec06 (B1)	-	-	-	-	-	-	-	0.2027	0.06 ± 0.02	-	11.5 (2)	KNSTD
BE24214	Blank1 06 Aug 07 (B2)	-	-	-	-	-	-	-	0.2021	0.07 ± 0.03	-	17.9 (3)	07KNSTD
BE24227	Blank2 06 Aug 07 (B3)	-	-	-	-	-	-	-	0.2015	0.05 ± 0.02	-	16.1 (3)	07KNSTD
BE21024	Blank 12 July 05 (B4)	-	-	-	-	-	-	-	0.2015	0.21 ± 0.05	-	29.5 (3)	KNSTD
BE28307	Blank1 08 Jan 10 (B5)	-	-	-	-	-	-	-	0.1821	0.08 ± 0.02	-	19.2 (2)	07KNSTD
BE28316	Blank2 08 Jan 10 (B6)	-	-	-	-	-	-	-	0.1830	0.03 ± 0.01	-	20.2 (2)	07KNSTD
BE28336	Blank1 31 Aug 09 (B7)	-	-	-	-	-	-	-	0.1817	0.12 ± 0.03	-	20.4 (2)	07KNSTD

[a] – Carrier ^{9}Be concentration is 996 ppm for all samples except KIWI 631, for which the carrier ^{9}Be concentration is 985 ppm.
[b] – $^{9}Be^{+3}$ measured after the accelerator. Reported currents are averaged over all AMS runs for a given sample. The number of AMS runs is given in parentheses.
[c] – AMS standards to which respective ratios and concentrations are referenced. Reported $^{10}Be/^{9}Be$ ratios for KNSTD and 07KNSTD are 3.15×10^{-12} and 2.85×10^{-12}, respectively[37]. Respective procedural blanks are indicated in subscript and refer to blanks given at bottom of table. Where two blanks are shown, the average was used to correct sample ratios in the respective sample batch.

DOI: 10.1038/NGEO962

Table S2. ^{10}Be surface-exposure ages (in kyrs ± 1σ) from the Birch Hill and mid-Macaulay moraines. One outlying age is italicized and excluded from landform mean and error (see Section 2.3 for details). SEM: standard error of the mean. PR: production rate uncertainty (2.1-2.2%[14]). Bold ages ('Lm') are those discussed in text.

Sample ID	St	De	Du	Li	Lm
'Outboard' Birch Hill ridge					
BH-07-08	14.04 ± 0.42	14.27 ± 0.43	14.26 ± 0.43	14.36 ± 0.43	**14.06 ± 0.42**
BH-07-09	14.09 ± 0.41	14.32 ± 0.42	14.31 ± 0.42	14.41 ± 0.42	**14.11 ± 0.41**
Mean ± 1σ	14.06 ± 0.04	14.29 ± 0.03	14.29 ± 0.03	14.38 ± 0.03	14.09 ± 0.03
Mean ± SEM	14.06 ± 0.02	14.29 ± 0.02	14.29 ± 0.02	14.38 ± 0.02	14.09 ± 0.02
Mean ± [SEM+PR]	14.06 ± 0.31	14.29 ± 0.32	14.29 ± 0.32	14.38 ± 0.31	**14.09 ± 0.30**
Birch Hill I ridge					
BH-06-02	12.99 ± 0.42	13.15 ± 0.42	13.13 ± 0.42	13.22 ± 0.43	**13.01 ± 0.42**
BH-06-03	12.41 ± 0.46	12.59 ± 0.47	12.58 ± 0.47	12.66 ± 0.47	**12.43 ± 0.46**
BH-06-04	12.43 ± 0.35	12.61 ± 0.36	12.60 ± 0.36	12.68 ± 0.36	**12.46 ± 0.35**
BH-06-05	12.46 ± 0.44	12.61 ± 0.45	12.59 ± 0.44	12.67 ± 0.45	**12.48 ± 0.44**
BH-06-06	12.99 ± 0.41	13.14 ± 0.41	13.12 ± 0.41	13.21 ± 0.41	**13.01 ± 0.41**
BH-06-07	12.67 ± 0.47	12.81 ± 0.48	12.79 ± 0.48	12.88 ± 0.48	**12.69 ± 0.47**
BH-07-10	12.58 ± 0.35	12.81 ± 0.35	12.81 ± 0.35	12.89 ± 0.36	**12.62 ± 0.35**
BH-07-11	*15.83 ± 1.58*	*16.05 ± 1.60*	*16.05 ± 1.60*	*16.14 ± 1.61*	***15.82 ± 1.58***
BH-07-12	12.93 ± 0.39	13.17 ± 0.39	13.16 ± 0.39	13.25 ± 0.40	**12.97 ± 0.39**
BH-07-13	13.45 ± 0.32	13.64 ± 0.32	13.63 ± 0.32	13.72 ± 0.32	**13.47 ± 0.32**
BH-07-14	13.40 ± 0.31	13.59 ± 0.31	13.58 ± 0.31	13.67 ± 0.31	**13.42 ± 0.31**
BH-07-15	13.14 ± 0.45	13.34 ± 0.46	13.32 ± 0.46	13.41 ± 0.46	**13.17 ± 0.45**
BH-07-16	13.41 ± 0.38	13.61 ± 0.39	13.59 ± 0.39	13.69 ± 0.39	**13.43 ± 0.38**
BH-07-17	12.92 ± 0.40	13.11 ± 0.41	13.09 ± 0.41	13.18 ± 0.41	**12.94 ± 0.41**
BH-07-18	13.44 ± 0.40	13.63 ± 0.40	13.61 ± 0.40	13.71 ± 0.40	**13.46 ± 0.40**
Mean ± 1σ	12.94 ± 0.39	13.13 ± 0.40	13.11 ± 0.39	13.20 ± 0.40	12.97 ± 0.39
Mean ± SEM	12.94 ± 0.10	13.13 ± 0.11	13.11 ± 0.11	13.20 ± 0.11	12.97 ± 0.10
Mean ± [SEM+PR]	12.94 ± 0.30	13.13 ± 0.31	13.11 ± 0.31	13.20 ± 0.31	**12.97 ± 0.30**
Birch Hill II recessional ridges					
BH-06-09	13.14 ± 0.74	13.35 ± 0.75	13.34 ± 0.75	13.43 ± 0.76	**13.17 ± 0.74**
BH-06-10	13.04 ± 0.43	13.26 ± 0.44	13.25 ± 0.44	13.35 ± 0.44	**13.07 ± 0.44**
BH-06-11	12.90 ± 0.40	13.12 ± 0.41	13.11 ± 0.41	13.20 ± 0.41	**12.93 ± 0.40**
BH-06-12	13.35 ± 0.51	13.56 ± 0.52	13.55 ± 0.52	13.65 ± 0.52	**13.37 ± 0.51**
BH-06-13	13.22 ± 0.43	13.44 ± 0.43	13.43 ± 0.43	13.53 ± 0.44	**13.25 ± 0.43**
KIWI-631	13.30 ± 0.35	13.53 ± 0.35	13.52 ± 0.35	13.61 ± 0.36	**13.33 ± 0.35**
KIWI-632	12.66 ± 0.28	12.88 ± 0.28	12.87 ± 0.28	12.96 ± 0.29	**12.69 ± 0.28**
Mean ± 1σ	13.08 ± 0.24	13.30 ± 0.23	13.29 ± 0.23	13.39 ± 0.23	13.12 ± 0.24
Mean ± SEM	13.08 ± 0.09	13.30 ± 0.09	13.29 ± 0.09	13.39 ± 0.09	13.12 ± 0.09
Mean ± [SEM+PR]	13.08 ± 0.29	13.30 ± 0.31	13.29 ± 0.31	13.39 ± 0.31	**13.12 ± 0.30**
'Mid-Macaulay' moraines (middle ridge)					
MR-09-01	13.33 ± 0.32	13.31 ± 0.31	13.24 ± 0.31	13.34 ± 0.32	**13.30 ± 0.31**
MR-09-02	13.21 ± 0.28	13.20 ± 0.28	13.13 ± 0.28	13.23 ± 0.28	**13.19 ± 0.28**
MR-09-03	13.47 ± 0.32	13.46 ± 0.32	13.39 ± 0.32	13.49 ± 0.32	**13.44 ± 0.32**
Mean ± 1σ	13.34 ± 0.13	13.32 ± 0.13	13.25 ± 0.13	13.34 ± 0.13	13.31 ± 0.13
Mean ± SEM	13.34 ± 0.08	13.32 ± 0.08	13.25 ± 0.07	13.34 ± 0.08	13.31 ± 0.08
Mean ± [SEM+PR]	13.34 ± 0.29	13.32 ± 0.29	13.25 ± 0.29	13.34 ± 0.29	**13.31 ± 0.29**

Table S3. Calendar-year age estimates for key late-glacial climate transitions and event durations as given by records mentioned in the main text. Uncertainties, where stated, are as reported in the original references. ^{10}Be ages denoted by * have been adjusted to years before CE1950 for direct comparison to radiocarbon calendar ages (See Supplementary Methods).

Location	Event	Record	Age (yrs)	Reference(s)
		NORTHERN HEMISPHERE		
75.1°N 42.3°W	Onset of YD cooling over Greenland	NGRIP ice core $\delta^{18}O$	12,890 ± 137	63,64
75.1°N 42.3°W	Onset of B-A in Greenland	NGRIP ice core $\delta^{18}O$	14,690 ± 185	63,64
75.1°N 42.3°W	Length of B-A in Greenland	NGRIP ice core $\delta^{18}O$	~1,800	64,65
		SOUTHERN HEMISPHERE		
36.7°S 136.6°E	Culmination of late-glacial sea-surface cooling south of Australia	Alkenone-inferred SSTs at MD03-2611	~13,270	66
41.0°S 74.5°W	Culmination of late-glacial cooling of water west of Chile	*G. bulloides* foraminiferal $\delta^{18}O$-inferred water temperatures at ODP core site 1233	~13,000	67
41.1°S 7.8°E	Culmination of late-glacial cooling of water in the South Atlantic	Occurrence of polar foraminiferal species in core TN057-21	~13,300	68
43.4°S 170.2°E	Advance of the Franz Josef Glacier, Westland, New Zealand	AMS ^{14}C dating of overrun wood at Canavans Knob	13,030 ± 40 (*n=38*)	46,47 (see Supplementary Methods)
43.6°S 170.6°E	Culmination of late-glacial advance of Macaulay glacier, New Zealand	^{10}Be surface-exposure mean age of mid-Macaulay moraine ridge	13,310 ± 290 * (*n*=3)	This study
43.8°S 170.1°E	Culmination of late-glacial advance of Pukaki glacier, New Zealand	^{10}Be surface-exposure mean age of Birch Hill I moraine ridge	12,970 ± 300 * (*n=15*)	This study
43.8°S 170.1°E	Recession of Pukaki glacier from late-glacial maximum position	^{10}Be surface-exposure mean age of Birch Hill II recessional moraine ridges	13,120 ± 300 * (*n=7*)	This study
43.8°S 170.1°E	Earliest detected late-glacial advance to Birch Hill position	Tentative ^{10}Be surface-exposure age of moraine ridge outboard of Birch Hill I ridge	14,090 ± 300 * (*n=2*)	This study
74.9°S 123.3°E	Culmination of ACR cooling over East Antarctica	EPICA Dome C Deuterium	12,760 ± 340	65,69
74.9°S 123.3°E	End of ACR atmospheric CO_2 pause	EPICA Dome C Carbon Dioxide	12,860 ± 100	69, placed on the NGRIP methane-synchronized timescale of ref. 65
74.9°S 123.3°E	Onset of ACR cooling over East Antarctica	EPICA Dome C Deuterium	14,540 ± 400	65,69
74.9°S 123.3°E	Beginning of ACR atmospheric CO_2 pause	EPICA Dome C Carbon Dioxide	14,600 ± 100	69, placed on the NGRIP methane-synchronized timescale of ref. 65
74.9°S 123.3°E	Length of ACR in Antarctica	EPICA Dome C Deuterium	~1,780	65